

# Cosmological mass functions and moving barrier models

Asim Mahmood<sup>1,2</sup> and R. Rajesh<sup>3</sup>

<sup>1</sup>*Astrophysics, Denys Wilkinson building, Keble Road, Oxford, OX1 3RH, UK*

<sup>2</sup>*Inter University Centre for Astronomy and Astrophysics, Pune, 411007, India*

<sup>3</sup>*Martin Fisher School of Physics, Brandeis University, Mailstop 057, Waltham, MA 02454-9110, USA*

## ABSTRACT

In the ellipsoidal collapse model, the critical density for the collapse of a gravitationally bound object is a function of its mass. In the excursion set formalism, this translates into a moving barrier problem such that the mass function of dark matter haloes is given by the first crossing probability of a random walker across the barrier. In this paper, we study this first crossing probability analytically. Complete solutions are obtained for barriers that vary as square root of time and square of time. Large and small time asymptotic behaviour is derived. For arbitrary power-law barriers, the large time behaviour is determined. The solutions allow us to derive useful inferences about the scaling of the conditional mass function in terms of present day halo masses and look back redshifts. As an application of our results, we compare the estimates of major merger rates of haloes in constant and moving barrier models and find that for massive haloes ( $10^{12-13}M_{\odot}$ ) the latter predicts significantly higher merger rates towards high redshifts ( $z \gtrsim 4$ ).

**Key words:** galaxies: clusters: general – cosmology: theory – dark matter.

## 1 INTRODUCTION

The problem of determining the mass function of gravitationally bound structures was first addressed in a successful manner by Press & Schechter (1974), whose model assumed that the primordial density fluctuations filtered on a given mass scale were Gaussian distributed. Since their model, many detailed schemes have been investigated and perfected. The excursion set approach developed in Bond et. al. (1991) (hereafter BCEK) and Lacey & Cole (1993) (hereafter LC93) is a convenient tool for deriving the unconditional and the conditional mass functions within the framework of Gaussian random fields. The approach has been successfully used to create Monte-Carlo merging history trees of dark matter haloes (Kauffmann, White & Guiderdoni 1993; Somerville & Kolatt 1999; Sheth & Lemson 1999). As compared to  $N$ -body simulations, Monte-Carlo merger trees provide alternative faster methods for studying the build-up of dark matter haloes. Mo & White (1996) further showed how the spatial distribution of haloes may be quantified within the excursion set approach.

The excursion set approach is based on the following principles. Consider a dark matter inhomogeneity centred around some point in the universe. The smoothed density contrast within a radius  $R$  around this point is defined as  $\bar{\delta}(R) = [\bar{\rho}(R) - \rho_0]/\rho_0$ , where  $\bar{\rho}(R)$  is the density of matter within  $R$  and  $\rho_0$  is the mean background density of the universe. If the density contrast is greater than the critical density for collapse, the matter contained within the

volume eventually collapses to form a bound object. Practically,  $\bar{\delta}(R)$  is obtained by convolving the matter density field with some spherically symmetric function  $W_R(r)$  of radial extent  $R$ . The variance of the smoothed density contrast is then (e.g., LC93)

$$S(R) = \langle |\bar{\delta}(R)|^2 \rangle = \frac{1}{2\pi^2} \int_0^\infty dk \langle |\delta_k|^2 \rangle \hat{W}_R^2(k) k^2, \quad (1)$$

where  $\delta_k$ 's are the Fourier amplitudes of the field and  $\hat{W}_R(k)$  is the Fourier transform of the window function  $W_R(r)$ .

A convenient choice for the window function is the sharp  $k$  space function, where the cutoff wavenumber  $k_s$  is related to the Lagrangian radius ( $R$ ) of an object by  $R \sim (9\pi/2)^{1/3} k_s^{-1}$  (LC93). The equivalent mass scale is  $M \sim \rho_0 R^3$ . The sharp  $k$  window function has the advantage that  $\bar{\delta}[R(k_s)]$  executes a random walk with every increment in the size of the window. The linearly extrapolated critical density for collapse now serves as an absorbing barrier for random walk trajectories and the mass function of collapsed objects is given by the first crossing distribution of these random walks across the barrier.

In the spherical collapse model, the critical density is independent of the collapsing halo masses. When linearly extrapolated to the present day, it has a value of  $\delta_c = 1.686$  in a standard Cold Dark Matter (CDM) universe. The mass function of dark matter haloes derived using the excursion set approach with spherical collapse model lie within 10 – 30 % of the results from  $N$ -body simulations (Jenkins et al. 2001). Detailed comparison of simula-

tions with analytical results shows discrepancies for both small and large mass haloes (Gelb & Bertschinger 1994; Lacey & Cole 1994; Tormen 1998; Sheth & Tormen 1999).

Sheth, Mo & Tormen (2001) (hereafter SMT01) and Monaco (1997a,b) investigated a non-spherical alternative for collapse of over-densities. In particular they focused on an ellipsoidal collapse scenario which derives support from the triaxial nature of perturbations in Gaussian density fields (Doroshkevich 1970; Bardeen et. al. 1986). They argued that the main effect of an ellipsoidal collapse is to introduce a dependence of the critical density on the halo mass. In the excursion set formalism this amounts to incorporating a ‘moving’ barrier instead of a fixed one.

In a subsequent paper Sheth & Tormen (2002) (hereafter ST02) presented a detailed discussion on moving barrier models. They considered random walks in one dimensions  $x [\equiv \bar{\delta}(k_s)]$  diffusing with time  $t [\equiv S(k_s)]$  starting at  $x = 0$  when  $t = 0$ . The first crossings with a moving barrier of the form  $B(t) = a + bt^\gamma$  were studied. Based on first crossing distributions  $f(t)$  obtained from Monte-Carlo simulations, they suggested that for a barrier  $B(t)$ ,  $f(t)$  has the form

$$f(t) = \frac{ae^{-B(t)^2/(2t)}}{\sqrt{2\pi}t^{3/2}} \left[ 1 + \frac{bt^\gamma}{a} \sum_{n=0}^{n^*} \frac{(-1)^n}{n!(\gamma-n)} \prod_{k=0}^n (\gamma-k) \right], \quad (2)$$

where  $n^* \sim 5$ . In this expression, the diffusion constant  $D$  has been set equal to 1. Equation 2, when specialised to constant ( $b = 0$ ) and linear barriers ( $\gamma = 1$ ), gives the correct answer. For these two barriers, the first passage distribution is easily obtained by the reflection principle (Feller 1970) and is

$$f(t) = \begin{cases} \frac{a}{t} \frac{1}{\sqrt{2\pi Dt}} \exp\left[-\frac{a^2}{2Dt}\right] & b = 0, \\ \frac{a}{t} \frac{1}{\sqrt{2\pi Dt}} \exp\left[-\frac{(a+bt)^2}{2Dt}\right] & \gamma = 1. \end{cases} \quad (3)$$

However, the validity of equation 2 for other kinds of barriers remains unchecked. For the two barrier problem, corresponding to the conditional mass function (the conditional mass function gives the progenitor mass distribution for a given present day halo at a given look-back redshift), further formulae were suggested based on a generalisation of the above expression.

The precise value of  $\gamma$  applicable to the ellipsoidal collapse model seems to lie between 0.5 and 1.0. Based on numerics and other arguments, SMT01 argue that  $\gamma \approx 0.6$  with  $b > 0$ . On the other hand, by applying Lagrangian perturbation theory and considering an ellipsoidal collapse model, Monaco (1997a,b) concludes that  $\gamma = 1/2$  with  $b < 0$ . Also, from the study of tidal torques on galaxy evolution Del Popolo & Gambera (1998) showed that barrier is of the form  $b > 0$  and  $\gamma \approx 0.58$  (Del Popolo 2002).

In this paper, we present an analysis of the first passage distribution  $f(t)$  for a random walker with a moving barrier. In the process we test the validity of equation 2. We present an analytical solution of the square root barrier ( $\gamma = 1/2$ ). This barrier is close to the one studied in SMT01 ( $\gamma \approx 0.6$ ). We also solve for the quadratic boundary ( $\gamma = 2$ ). The large and small time behaviour of these solutions are also derived. For arbitrary  $\gamma$ , we calculate the large time behaviour of the first crossing probability. Our results show that equation 2 is not correct in general and needs to be modified.

We also present the methodology for approaching the problem of conditional mass functions in the context of moving barrier models. The conditional mass function requires solving a two barrier problem. Section 2 describes how to modify the moving barrier problem so that both the conditional as well as unconditional mass distributions may be obtained.

The rest of the paper is organised as follows. In section 3, we present the analytical solution for the square root barrier ( $\gamma = 1/2$ ). The large and small time asymptotic behaviour is derived. Expressions are also obtained for conditional mass distributions. The analytical results are compared with results from Monte-Carlo simulations.

In section 4, we consider another solvable limit – the quadratic barrier ( $\gamma = 2$ ). The full solution and the large time asymptotic behaviour are derived, and compared with results from simulations. For both these cases, we show that the results are not consistent with the formula in equation 2.

In section 5, we consider barriers with arbitrary  $\gamma$ . For this general case, we argue what the large time behaviour of  $f(t)$  should be. Using special algorithms, we numerically obtain  $f(t)$  for large times and confirm our prediction.

In section 6 we fit the halo mass distribution obtained from  $N$ -body simulations with the square root barrier results. While a good fit is obtained, the numerical data is not good enough to differentiate between different values of  $\gamma$ .

In section 7, we describe an application of the results to estimate major merger rates of haloes. These rates are calculated using the conditional mass functions for the square root barrier. These rates are compared with those derived from a constant barrier Press-Schechter model. The analysis suggests that while the two models are very similar in describing the low redshift evolution of these rates, there is a systematic deviation to wards high redshifts. In particular the cumulative major merger rates of massive haloes ( $10^{12-13} M_\odot$ ) differ significantly at redshifts  $z \gtrsim 4$ .

We conclude with a summary and discussion in Section 8. In Appendix A, results for parabolic cylinder functions that are relevant to the paper are reproduced.

Unless otherwise stated, the cosmological parameters used will be  $\Omega_m = 0.3$ ,  $\Omega_\Lambda = 0.7$ ,  $h = 0.7$  and root mean square fluctuations at  $8 h^{-1} \text{Mpc}$  as  $\sigma_8 = 0.9$ . We also interchangeably use  $x \leftrightarrow \delta$  and  $t \leftrightarrow S$ .

## 2 THE MOVING BARRIER MODEL

For the ellipsoidal collapse model, the critical density contrast depends on the variance or ‘scale’  $S$  and has the form (Sheth, Mo & Tormen 2001)

$$\delta_{ec}(S, z) = \sqrt{q} \delta_{sc}(z) \left[ 1 + \beta \left( \frac{S}{qS_*} \right)^\gamma \right]. \quad (4)$$

Here,  $\delta_{sc}(z)$  is the spherical collapse critical density at redshift  $z$  and  $S_* = \delta_{sc}^2(z)$ . The best-fit values of parameters  $\beta$ ,  $\gamma$  and  $q$  for the mass function of haloes in GIF simulations of the Virgo consortium (Jenkins et al. 1998) are 0.5, 0.6 and 0.707 respectively. The value of  $q$  depends on the way haloes are identified in the simulations and therefore is a function of the link-length in the halo finding algorithms.

The variable  $\delta$  executes a random walk when  $S$  is increased. We are interested in the probability that  $\delta$  exceeds

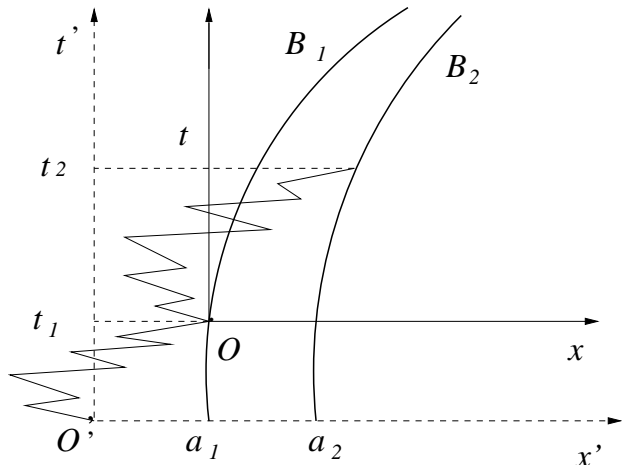


**Figure 1.** Illustration of the two barrier problem corresponding to the conditional mass distribution.

the critical density  $\delta_{ec}$  at scale  $S$ . In the following analysis it is convenient to substitute the variables  $\delta$  and  $S$  by variables  $x$  and  $t$  respectively. Consider a random walk starting at  $x = 0$  when  $t = 0$ . Let  $P(x, t)$  be the probability of finding it at  $x$  at time  $t$ . Then,  $P(x, t)$  obeys the diffusion equation

$$\frac{\partial P(x, t)}{\partial t} = \frac{D}{2} \frac{\partial^2 P(x, t)}{\partial x^2}, \quad (5)$$

where  $D$  is the diffusion constant with a value one in the present context. In terms of  $x$  and  $t$ , the barrier in equation 4 takes the form  $a + bt^\gamma$ , where  $a, b$  are constants.

In what follows, we will consider modified barriers of the form

$$B(t) = a + b(t + t_0)^\gamma, \quad (6)$$

where  $t_0$  is some constant (see below for motivation for this choice). Let  $g(a, b, t_0; t)$  be the probability that the random walk crosses the barrier  $B(t)$  for the first time at time  $t$ . The unconditional mass distribution is obtained by setting  $t_0 = 0$ . To calculate the conditional mass function one has to consider a two barrier problem.

Consider the illustration in figure 1. The random walk trajectories begin at position  $O'$ . The moving barrier  $B_1$  represents the critical density at present epoch  $z_1$  and has the form  $B_1 \equiv a_1 + b_1 t_1^\gamma$ . At an earlier epoch  $z_2$  the critical density is represented by barrier  $B_2 \equiv a_2 + b_2 t_2^\gamma$ . For earlier look-back epochs or redshifts (increasing  $z$ ),  $a_2 > a_1$ . The precise dependence of  $a$  on  $z$  is determined from the cosmological model. For example, in an  $\Omega_m = 1$  universe  $a_{1,2} = 1.686 \times (1 + z_{1,2})$  [Note: the parameter  $a$  should not be confused with the scale factor which is often represented by the same notation].

The jagged curve shows a random walk trajectory that meets the barrier  $B_1$  for the first time at some scale  $t_1$  and the barrier  $B_2$  for the first time at some ‘smaller’ scale  $t_2$ . This represents a collapsed object of scale  $t_1$  at redshift  $z_1$  that had a collapsed (or ‘formed’) progenitor of scale  $t_2$  at redshift  $z_2$ . Let  $f(t_1 \cap t_2)$  be the probability of this occurring. To determine  $f(t_1 \cap t_2)$ , we need to know the probability that a random walk starting at the point  $O$  reaches the barrier  $B_2$  for the first time in time  $t_2 - t_1$ . In the new coordinates  $x, t$ , the barrier takes the form  $a + b(t + t_1)^\gamma$ ,

where  $a = a_2 - a_1 - b_1 t_1^\gamma$  and  $b = b_2$ . Thus,

$$f(t_1 \cap t_2) = g(a_1, b_1, 0; t_1) g(a_2 - a_1 - b_1 t_1^\gamma, b_2, t_1; t_2 - t_1). \quad (7)$$

The conditional mass distribution  $f(t_2|t_1)$  is then given by

$$f(t_2 | t_1) = g(\Delta a - b_1 t_1^\gamma, b_2, t_1; t_2 - t_1), \quad (8)$$

where  $\Delta a = a_2 - a_1$ . Thus, a knowledge of  $g(a, b, t_0; t)$  solves both the conditional as well as unconditional mass distributions. This was the motivation for introducing the parameter  $t_0$  into the modified barrier. In what follows, we will be considering the case when  $b_1 = b_2 = b$ .

The first step in solving equation 5 is to make the boundary condition (equation 6) time independent by choosing suitable coordinates. Let  $x \rightarrow B_1(t) - x$ , with  $t$  remaining unchanged. Then, equation 5 reduces to

$$\frac{\partial P(x, t)}{\partial t} + b\gamma(t + t_0)^{\gamma-1} \frac{\partial P(x, t)}{\partial x} - \frac{D}{2} \frac{\partial^2 P(x, t)}{\partial x^2} = 0, \quad (9)$$

satisfying the boundary conditions

$$P(0, t) = 0, \quad (10)$$

$$P(\infty, t) = 0, \quad (11)$$

$$P(x, 0) = \delta_D[x - (a + bt_0^\gamma)], \quad (12)$$

where  $\delta_D$  is the Dirac delta function. The first crossing distribution is

$$g(a, b, t_0; t) = -\frac{\partial}{\partial t} \int_0^\infty P(x, t) dx. \quad (13)$$

$$= \frac{D}{2} \left[ \frac{\partial P}{\partial x} \right]_{x=0}, \quad (14)$$

where the integral in equation 13 has been evaluated using equation 9.

We now bring equation 9 to a more convenient form by the following transformations. Let  $P(x, t) = \phi(x, t)e^{h(x, t)}$ . Substituting into equation 9, we determine the function  $h(x, t)$  by eliminating the terms proportional to  $\partial\phi/\partial x$ . Thus, if we choose  $h(x, t)$  to be

$$h(x, t) = \frac{b\gamma x(t + t_0)^{\gamma-1}}{D} - \frac{b^2\gamma^2(t + t_0)^{2\gamma-1}}{2D(2\gamma-1)}, \quad \gamma \neq \frac{1}{2}, \quad (15)$$

then equation 9 simplifies to

$$\frac{\partial\phi}{\partial t} + \frac{b\gamma(\gamma-1)x}{D(t+t_0)^{2-\gamma}}\phi - \frac{D}{2} \frac{\partial^2\phi}{\partial x^2} = 0, \quad \gamma \neq \frac{1}{2}. \quad (16)$$

When  $\gamma = 2$ , the second term in equation 16 becomes independent of time, and the equation becomes separable. We present the full solution for this case in section 4. Also, it turns out that when  $\gamma = 1/2$ , the equation 9 can be made separable by a different set of transformations. We present the complete solution for this case in section 3. For arbitrary  $\gamma$ , it is not possible to transform equation 16 into a separable form. However, it is possible to derive some results in the limit of large time. We discuss this in section 5.

### 3 THE SQUARE ROOT BARRIER

In this section we solve for the first crossing probability for the square root barrier ( $\gamma = 1/2$ ).

### 3.1 Solution

Let  $y = x/\sqrt{t+t_0}$  and  $\eta = t$ . Then equation 9 simplifies to

$$(\eta + t_0) \frac{\partial P}{\partial \eta} + \frac{b-y}{2} \frac{\partial P}{\partial y} - \frac{D}{2} \frac{\partial^2 P}{\partial y^2} = 0. \quad (17)$$

Equation 17 is now separable. Let  $P(y, \eta) = \Theta(\eta)\Psi(y)$ . Then,

$$\frac{(\eta + t_0)}{\Theta(\eta)} \frac{\partial \Theta}{\partial \eta} = -\lambda \quad (18)$$

$$\frac{D}{2\Psi} \frac{\partial^2 \Psi}{\partial y^2} + \frac{(y-b)}{2\Psi} \frac{\partial \Psi}{\partial y} = +\lambda, \quad (19)$$

where  $\lambda$  is an eigenvalue. The first of these equations is easily integrated to give

$$\Theta(\eta) = \frac{1}{(\eta + t_0)^\lambda}. \quad (20)$$

In equation 19, we substitute  $(y-b)/\sqrt{D} = \zeta$ . Then,

$$\Psi(\zeta)'' + \zeta\Psi(\zeta)' + 2\lambda\Psi(\zeta) = 0. \quad (21)$$

Further, letting  $2\lambda - 1 = v$ , and applying a transformation  $\Psi(\zeta) = \Phi(\zeta) \exp(-\zeta^2/4)$ , we obtain

$$\Phi''(\zeta) + (v + \frac{1}{2} - \frac{1}{4}\zeta^2)\Phi(\zeta) = 0. \quad (22)$$

The solutions to this equation are the parabolic cylinder functions  $U_v(\zeta)$  and the eigen values  $v$  are determined by the boundary condition  $U_v(-b/\sqrt{D}) = 0$  (from equation 10). For large  $\zeta$ , the function  $U_v(\zeta)$  goes to zero as  $\zeta^v \exp(-\zeta^2/4)[1 + O(1/\zeta)]$ , consistent with the other boundary condition.

It is interesting to note a similarity between the present problem and the problem of a quantum particle trapped in a potential  $V(\zeta)$  given as

$$V(\zeta) = \begin{cases} \infty, & \zeta \leq -\frac{b}{\sqrt{D}}, \\ \frac{1}{4}\zeta^2, & \zeta > -\frac{b}{\sqrt{D}}. \end{cases} \quad (23)$$

In the limit  $b = 0$ , the problem reduces to the harmonic oscillator potential with an  $V(\zeta) = \infty$  for  $\zeta \leq 0$ . The parabolic cylinder functions then reduce to Hermite polynomials with  $U_{2n+1}(z) = 2^{-n-1/2} H_{2n+1}(z) e^{-z^2/4}$ .

For finite  $b$  exact eigen-values can be obtained numerically. Alternatively, the large  $n$  behaviour of  $v_n$  may be obtained from the large  $v$  asymptotic behaviour of the parabolic cylinder function (see appendix A). Then,

$$v_n = 2n - \frac{2\sqrt{2}b}{\pi\sqrt{D}}\sqrt{n} + \frac{2b^2}{\pi^2 D} + (2k-1) + O\left(\frac{1}{\sqrt{n}}\right), \quad n \rightarrow \infty, \quad (24)$$

where  $k$  is an integer.

The probability  $P(x, t)$  can now be written as a linear combination of all eigen modes as

$$P(x, t) = \sum_n \frac{A_{v_n}}{(t+t_0)^{(v_n+1)/2}} U_{v_n} \left( \frac{x - b\sqrt{t+t_0}}{\sqrt{D(t+t_0)}} \right) \times \exp \left[ -\frac{(x - b\sqrt{t+t_0})^2}{4D(t+t_0)} \right]. \quad (25)$$

Here  $A_{v_n}$  are constants that are determined through the initial condition. Using the orthogonality relation for parabolic cylinder functions

$$\int_{-b/\sqrt{D}}^{\infty} U_\mu(\zeta) U_\nu(\zeta) d\zeta = 0, \quad \mu \neq \nu. \quad (26)$$

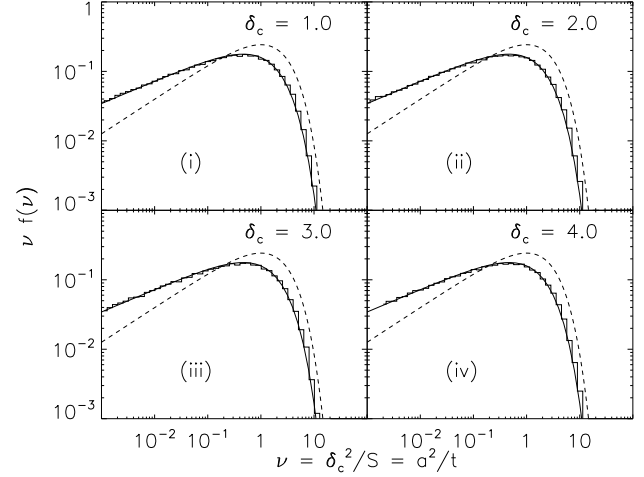


**Figure 2.** The unconditional mass function or the first crossing distribution for  $\gamma = 1/2$  (solid line) is compared with results from Monte Carlo simulations (histogram) for different values of  $\delta_c$ . The dashed curve is the mass function obtained from the Press-Schechter constant barrier model.

and using the initial condition 12, one obtains

$$A_\mu = \frac{t_0^{\mu/2} e^{a^2/(4Dt_0)}}{\sqrt{D} I_\mu(-b/\sqrt{D})} U_\mu \left( \frac{a}{\sqrt{Dt_0}} \right), \quad (27)$$

where we have defined  $I_\mu(-b/\sqrt{D})$  as

$$I_\mu \left( \frac{-b}{\sqrt{D}} \right) = \int_{-b/\sqrt{D}}^{\infty} U_\mu^2(\zeta) d\zeta. \quad (28)$$

Having obtained  $P(x, t)$ , we can derive the distribution  $g(a, b, t_0; t)$  in a straightforward manner using equation 14:

$$g(a, b, t_0; t) = \frac{e^{-b^2/(4D)} e^{a^2/(4Dt_0)}}{2(t+t_0)} \times \sum_{\{v\}} \left( \frac{t_0}{t+t_0} \right)^{v/2} \frac{U'_v(-b/\sqrt{D}) U_v(a/\sqrt{Dt_0})}{I_v(-b/\sqrt{D})}, \quad (29)$$

where  $U'_v(x)$  denotes a first derivative with respect to  $x$ . The conditional first crossing distribution can be obtained by using equation 8. To obtain the unconditional distribution we take the limit  $t_0 \rightarrow 0$  in equation 29 to obtain

$$g(a, b, 0; t) = \frac{\exp(-b^2/4D)}{2t} \sum_v \left( \frac{a^2}{Dt} \right)^{v/2} \frac{U'_v(-b/\sqrt{D})}{I_v(-b/\sqrt{D})}. \quad (30)$$

It is straightforward to show that one recovers the constant barrier answer from this expression by setting  $b = 0$ .

In figure 2, we compare the analytical result for unconditional mass function (equation 30) with results from Monte-Carlo simulations. In terms of the barrier form given in equation 4, the parameter values are  $\gamma = 0.5$ ,  $\beta = 0.5$  and  $q = 1$ . In the four panels (i, ii, iii and iv),  $a = \delta_{sc}(z) = 1, 2, 3$  and 4 respectively. The solid curve is obtained by truncating the series in equation 30 to the first 30 terms. There is a marked difference between the moving barrier and the constant barrier especially for large times (or small masses).

We also compare the expression for the square root barrier with Monte Carlo simulations for a  $\gamma = 0.6$  barrier.

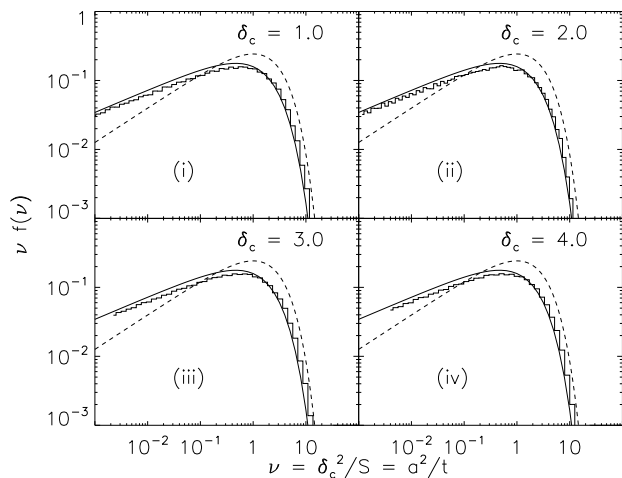


**Figure 3.** Same as in figure 2 except that the histogram is now for  $\gamma = 0.6$ .

This is shown in figure 3 where the solid curve is the expression in equation 30 and the histogram is data for  $\gamma = 0.6$ . The other parameters are same for both simulation and the curve. It is seen that the data lies close to the curve. In fact, if the parameters  $b$  and  $a$  were allowed to be played with, a much better fit can be obtained. This shows the difficulty in distinguishing between various  $\gamma$ 's by looking at the mass distribution.

### 3.2 Large time behaviour of the unconditional first crossing probability

In this subsection, we consider the large time behaviour of the first crossing probability. In the large time limit, the leading order contribution arises from the first term in the infinite series in equation 30. This corresponds to the variable  $\nu = a^2/(Dt) \rightarrow 0$  limit. The unconditional first crossing distribution behaves as  $f(t) \sim t^{-\theta}$  with  $\theta = 1 + v_0/2$ , where  $v_0$  is the smallest eigenvalue. It is not possible to analytically calculate  $v_0$  for arbitrary  $b$ . When  $b \rightarrow \infty$ , the eigenvalue problem reduces to the harmonic oscillator problem with lowest eigenvalue being 0. Thus one expects  $\theta \rightarrow 1$  as  $b \rightarrow \infty$ . When  $b \rightarrow -\infty$ , the barrier crosses the walker almost immediately. Thus, one expects that  $\theta \rightarrow \infty$  when  $b \rightarrow -\infty$ . For small  $b$  ( $b^2 \ll D$ ), using the variational method, Krapivsky & Redner (1996) obtained an approximate value of the exponent as  $\theta \approx 3/2 - b/\sqrt{2\pi D}$ . At the same time, one could naively assume that the large  $v$  behaviour for parabolic cylinder functions (see equation A2) is valid for all  $v$  and then estimate  $v_0$ . Under this assumption, one obtains

$$\theta = \frac{3}{2} - \frac{b}{\pi^2 D} \sqrt{b^2 + \pi^2 D} + \frac{b^2}{\pi^2 D}. \quad (31)$$

Surprisingly, this expression agrees very well with the real answer and also has the right limits for large absolute values of  $b$ . Figure 4 plots the behaviour of the exponent  $\theta$  as a function of  $b/\sqrt{D}$ . This scaling is markedly different from the fixed barrier scaling in large time limit  $f(t) \propto t^{-3/2}$ .

We mention here that, if we were to look at the large time behaviour of  $f(t)$  in equation 2 with  $\gamma = 1/2$ , then

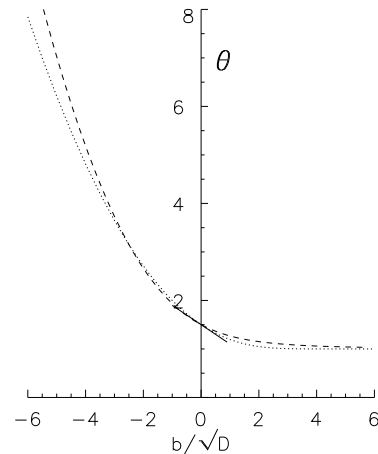


**Figure 4.** The variation of the exponent  $\theta$  with  $b/\sqrt{D}$  is shown for the square root barrier. The dotted line is obtained by numerically solving  $U_v(-b/\sqrt{D}) = 0$  for  $v$ ; the solid line shows the exponent obtained by Krapivsky & Redner (1996) and the dashed line is from equation 31. As expected, when  $b/\sqrt{D} = 0$ , the value of the exponent is  $3/2$ .

$\theta = 3/2 - \gamma = 1$ . Clearly, the lack of dependence on the parameter  $b$  makes it qualitatively different from the actual answer.

### 3.3 Small time behaviour of the unconditional first crossing probability

In the small time limit [ $\nu = a^2/(Dt) \gg 1$ ], we can determine the asymptotic behaviour of the first crossing probability  $g(a, b, 0; t)$  by the saddle point method. In this limit, the leading contribution to  $g(a, b, 0; t)$  comes from a term with large  $v$  in the infinite series of equation 30. On substituting the large  $v$  asymptotic form of functions  $U'_v$  and  $I_v$  (see Appendix A), and replacing the summation by an integral over  $n$  by noting from equation A3 that  $dn = [1/2 + b/(2\pi\sqrt{vD})]dv$ , equation 30 reduces to

$$f(t) = \frac{\exp(-b^2/4D)}{2\pi t \sqrt{2}} \int_0^\infty dv \left\{ \left( \frac{a^2}{Dt} \right)^{v/2} \left( \frac{e}{v} \right)^{v/2} \times \sin \left( \frac{\pi v}{2} + \frac{b\sqrt{v}}{\sqrt{D}} \right) [1 + O(1/v)] \right\}. \quad (32)$$

Here we have only retained terms up to  $O(1/\sqrt{v})$ . Rewriting the ‘sine’ term as an exponential, and evaluating the integral by the saddle point method, we obtain, after some algebra, the small time asymptotic form of the expression as

$$f(t) = \frac{a}{\sqrt{2\pi D} t^{3/2}} \exp \left[ -\frac{(a + b\sqrt{t})^2}{2Dt} \right] \times \left[ 1 + \frac{b(b^2 + 6D)\sqrt{t}}{24Da} + O \left( \frac{Dt}{a^2} \right) \right]. \quad (33)$$

Comparing this expression with equation 2, it appears that the latter should be considered as an expansion for the small time behaviour of  $f(t)$ . Specialising to  $\gamma = 1/2$ ,  $f(t)$  has the same form as in equation 33 except for the coefficient in front of the correction term. But whether this qualitative similarity continues to exist for  $\gamma > 1/2$  is not very clear. In

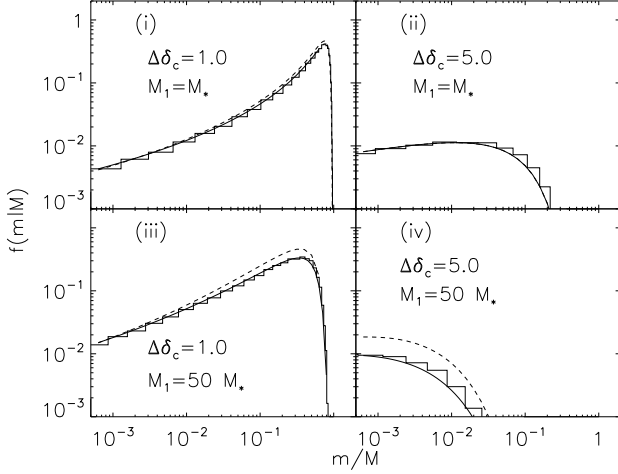


**Figure 5.** The analytical conditional mass function (solid curve) is compared with the results from Monte-Carlo simulations (histograms). The dashed curve is the fixed barrier conditional mass function. In panel (ii), the two curves are not distinguishable from each other. Here  $M_1$  is such that  $t_1 = S(M_1)$ .

fact, in sections 4 and 5, we will show that equation 2 does not have the right form for arbitrary  $\gamma$ .

### 3.4 Asymptotic analysis of the conditional mass function

In this subsection, we study the asymptotic behaviour of the conditional mass distribution. This is given by equation 8. Using the result for  $g(a, b, t_0; t)$  (see equation 29), we obtain

$$f(t_2 | t_1) = \frac{1}{2t_2} \exp \left[ \frac{(\Delta a)^2}{4Dt_1} - \frac{b\Delta a}{2D\sqrt{t_1}} \right] \times \sum_{\{v\}} \left( \frac{t_1}{t_2} \right)^{v/2} \frac{U'_v(-b/\sqrt{D}) U_v[(\Delta a - b\sqrt{t_1})/\sqrt{Dt_1}]}{I_v(-b/\sqrt{D})}, \quad (34)$$

where  $\Delta a = a_2 - a_1$ . Unlike the fixed barrier case, the conditional mass function is no longer a universal function of just one scaling variable  $\nu = \Delta a/\sqrt{t_2 - t_1}$ .

In figure 5, the conditional mass function as obtained from equation 34 (solid curve), is plotted with the results from Monte-Carlo simulations (histograms) for a range of present day halo masses ( $M_1$ ) and look-back redshifts. Here  $M_*$  is such that  $S(M_*) = \delta_{sc}^2(0)$ , which, for  $\Lambda$ CDM cosmology used here, has a value  $M_* \sim 2 \times 10^{13} M_\odot$ . The plot confirms the correctness of our expression. The result from the constant barrier model is shown for comparison (dashed curve). In figure 6 we show the effect of rescaling the conditional mass function in terms of variable  $\nu$ . As expected, the shape of the curve is different at different look-back epochs and for different present day halo masses.

We will consider the following limiting cases. Consider the limit  $(\Delta a/\sqrt{Dt_1}) \rightarrow \infty$ . This is the same limit as the one that was taken to obtain the unconditional mass distribution. Doing so, one obtains

$$\lim_{\frac{\Delta a}{\sqrt{Dt_1}} \rightarrow \infty} f(t_2 | t_1) = \frac{e^{-b^2/(4D)}}{2t_2} \sum_v \left( \frac{\Delta a^2}{Dt_2} \right)^{v/2} \frac{U'_v(-b/\sqrt{D})}{I_v(-b/\sqrt{D})}, \quad (35)$$

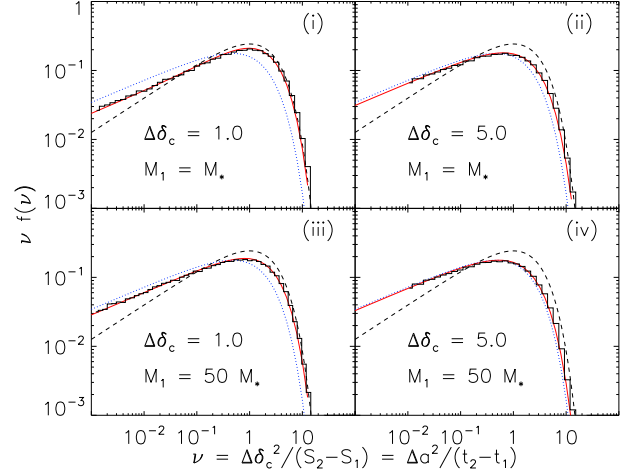


**Figure 6.** The conditional mass function plotted in terms of variable  $\nu = \Delta a^2/(t_2 - t_1)$ . The histograms show the results of Monte-Carlo simulations. The dotted curve shows the distribution obtained by re-scaling of the unconditional mass function. The dashed curve is the constant barrier mass function.

which is the same as equation 30 with  $a$  replaced by  $\Delta a$ . Therefore, for a given look back epoch, the conditional mass function tends to the unconditional mass function for large present epoch masses. Alternatively, for a fixed present epoch mass, the conditional distribution tends to the unconditional distribution at large look back epochs.

We now consider the opposite limit  $(\Delta a/\sqrt{Dt_1}) \rightarrow 0$ . Taking the Taylor series expansion of the function  $U(\Delta a/\sqrt{Dt_1} - b/\sqrt{D})$  we can write

$$U_v \left[ \frac{\Delta a - b\sqrt{t_1}}{\sqrt{Dt_1}} \right] \approx U_v(-b/\sqrt{D}) + \frac{\Delta a}{\sqrt{Dt_1}} U'_v(-b/\sqrt{D}), \quad (36)$$

where we have only taken terms up to order  $\Delta a/\sqrt{Dt_1}$ . Note that the first term on the right hand side is zero from the boundary condition. Thus equation 34 can be written as

$$f(t_2 | t_1) = \frac{\Delta a}{\sqrt{Dt_1}} \frac{1}{2t_2} \sum_{\{v\}} \left( \frac{t_1}{t_2} \right)^{v/2} \frac{U'_v(-b/\sqrt{D})^2}{I_v(-b/\sqrt{D})}. \quad (37)$$

In this limit there does not appear to be a direct way of discerning the behaviour of  $f(t_2 | t_1)$ . However, figure 6 suggests that the form of the conditional mass function in this limit is closer to the constant barrier mass function. This point has also been discussed in ST02: for a given  $t_1$ , at small look back epochs most random walkers will reach the second barrier in a relatively short time so that the barrier hasn't moved much and is effectively fixed. ST02 argue that the effect should be more pronounced for massive haloes. Instead, panels (i) and (iii) of figure 6 suggest that for small mass haloes the conditional distribution are more like the constant barrier distribution, whereas for more massive haloes, the conditional distribution tends to the unconditional distribution. Within the context of the present analysis, this may be understood by noting that for a given  $\Delta a$ , as  $M_1 \rightarrow \infty$  or equivalently  $t_1 \rightarrow 0$ , equation 34 approaches the unconditional mass function. A simple argument can also be put forward by looking at the barrier form under consideration:  $B \equiv \Delta a - b(t_1^{\gamma} - t_2^{\gamma})$  [see section 2]. When  $t_2 \rightarrow t_1$  (note that the minimum value of  $t_2$  is  $t_1$ ) the situation is similar to

the fixed barrier case. On the other hand when  $t_2 \gg t_1$ , the situation is similar to the single barrier problem. Therefore, for a given present halo mass and look back redshift, one expects a transition from a fixed barrier distribution to the unconditional moving barrier distribution.

#### 4 THE QUADRATIC BARRIER

In this section, we solve for the first passage distribution for the quadratic barrier ( $\gamma = 2$ ). We start with equation 16, which when specialised to  $\gamma = 2$  is

$$\frac{\partial \phi}{\partial t} + \frac{2bx}{D} \phi - \frac{D}{2} \frac{\partial^2 \phi}{\partial x^2} = 0. \quad (38)$$

Let  $\phi(x, t) = \psi(x)T(t)$ . Then,

$$\frac{1}{T} \frac{\partial T}{\partial t} = -\lambda, \quad (39)$$

$$\frac{2b}{D} x - \frac{D}{2\psi} \frac{\partial^2 \psi}{\partial x^2} = +\lambda, \quad (40)$$

where  $\lambda$  is an eigenvalue.

The time dependent part has a solution  $T(t) = e^{-\lambda t}$ . Let  $y = k(2bx/D - \lambda)$ , where

$$k = [D/(2b^2)]^{1/3}. \quad (41)$$

Then equation 40 reduces to the Airy equation

$$\frac{\partial^2 \psi}{\partial y^2} - y\psi = 0. \quad (42)$$

The solution to the above equation are Airy functions  $Ai(y)$  such that when  $y \rightarrow \infty$ ,  $Ai(y) \rightarrow 0$ . The other boundary condition  $\psi(x = 0) = 0$  implies  $Ai(-k\lambda) = 0$  and this fixes the eigen values  $\lambda_n$ . Hence, we can write solution in the form

$$\phi(x, t) = \sum_{n=1}^{\infty} C_n e^{-\lambda_n t} Ai \left[ k \left( \frac{2bx}{D} - \lambda_n \right) \right], \quad (43)$$

where the coefficients  $C_n$  are to be determined from the initial condition.

The function  $P(x, t)$  can now be written as

$$P(x, t) = \sum_{n=1}^{\infty} C_n \exp \left[ -\lambda_n t + \frac{2bxt}{D} - \frac{2b^2 t^3}{3D} \right] Ai \left[ k \left\{ \frac{2bx}{D} - \lambda_n \right\} \right]. \quad (44)$$

The initial condition now gives us

$$\delta_D(x - a) = \sum_{n=1}^{\infty} C_n Ai \left[ k \left( \frac{2bx}{D} - \lambda_n \right) \right]. \quad (45)$$

Multiplying both sides of this equation by  $Ai \left[ k \left( \frac{2bx}{D} - \lambda_m \right) \right]$  and integrating between the boundaries  $x = 0$  and  $x = \infty$ , we obtain, using the orthogonality of Airy functions,

$$Ai \left[ k \left( \frac{2ba}{D} - \lambda_m \right) \right] = C_m \int_0^{\infty} dx Ai'^2 \left[ k \left( \frac{2bx}{D} - \lambda_m \right) \right]. \quad (46)$$

The integral on the right hand side can be evaluated using the relation  $Ai''(x) = xAi(x)$  and is equal to:  $\frac{D}{2bk} Ai'^2(-k\lambda_m)$ , where  $Ai'$  is the derivative of the Airy function. Thus we obtain the coefficients as

$$C_m = \frac{2bk}{D} \frac{1}{Ai'^2(-k\lambda_m)} Ai \left[ k \left( \frac{2ba}{D} - \lambda_m \right) \right]. \quad (47)$$

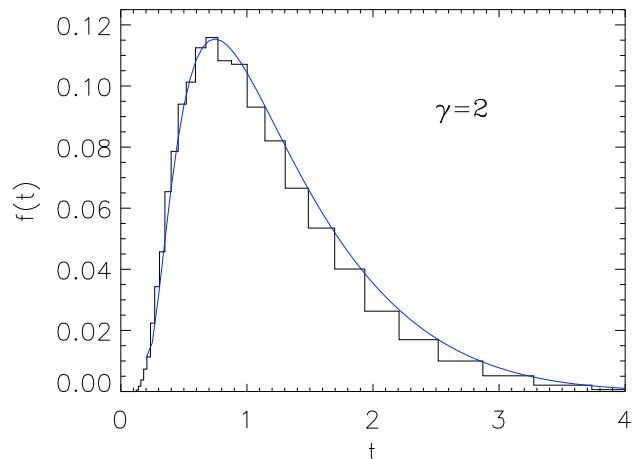


**Figure 7.** The unconditional first crossing probability for a quadratic barrier. The fiducial values of parameters are  $b = 0.2$  and  $a = 1.675$ . The solid curve is from equation 48 and histograms are from Monte-Carlo simulation of random walks.

Now using equation 14 we can write the expression for the first crossing distribution as

$$f(t) = \frac{2b^2 k^2 e^{-2b^2 t^3/(3D)}}{D} \sum_{n=1}^{\infty} e^{-\lambda_n t} \frac{Ai(2ba/D - \lambda_n)}{Ai'(-k\lambda_n)}. \quad (48)$$

Furthermore, the asymptotic form of the function  $Ai(-x)$  for  $x \rightarrow \infty$  is given as

$$Ai(-x) = \frac{1}{\sqrt{\pi x^{1/4}}} \sin \left( \frac{2}{3} x^{3/2} + \frac{\pi}{4} \right), \quad x \rightarrow \infty. \quad (49)$$

Thus using  $Ai(-k\lambda_n) = 0$ , we obtain the eigen values as

$$\lambda_n = \frac{1}{k} \left[ \frac{3\pi}{2} \left( n - \frac{1}{4} \right) \right]^{2/3}, \quad n \rightarrow \infty. \quad (50)$$

In the large time limit  $t \rightarrow \infty$  it can be seen that the leading order term in the first crossing distribution is  $f(t) \propto \exp[-2b^2 t^3/(3D)]$ . This can be compared with the expression in equation 2:  $f(t) \propto \exp[-b^2 t^3/(2D)]$ . Thus, when  $\gamma = 2$ , the expression by ST02 is wrong. Figure 7 shows the first crossing distribution for  $\gamma = 2$  for fiducial parameter values:  $b = 0.2$  and  $a = 1.675$ . The solid curve shows the result from equation 48 and the histograms show the distribution obtained from Monte-Carlo simulations.

#### 5 ARBITRARY $\gamma$

For  $\gamma$  different from 0, 1/2, 1, 2, it is not possible to obtain the full solution for  $f(t)$ . However, it is possible to analyse it in the limit of large  $t$ . This analysis would be useful to test whether equation 2 has the right form or not. In this section we estimate

$$\alpha = \lim_{t \rightarrow \infty} \frac{\ln(f(t))}{t^{2\gamma-1}}, \quad (51)$$

such that  $f(t) \propto \exp(\alpha t^{2\gamma-1})$ . For comparison, equation 2 gives  $\alpha = -b^2/2$ .

We start with equation 16 with  $t_0 = 0$ .  $\phi(x, t)$  obeys

the boundary condition  $\phi(0, t) = 0$ . The first passage distribution  $f(t)$  is then given by

$$f(t) = \frac{D}{2} \frac{\partial \phi}{\partial x} \Big|_{x=0} \exp \left[ \frac{-b^2 \gamma^2 t^{2\gamma-1}}{2D(2\gamma-1)} \right]. \quad (52)$$

We will argue that the contribution from  $\partial \phi / \partial x|_{x=0}$  is at an order much smaller than the term in the exponential in the limit  $t \rightarrow \infty$ .

For large  $t$ , one could treat the potential in equation 16 as a slowly varying linear potential. We then make the adiabatic approximation. As  $t \rightarrow \infty$ , we expect the system to be in ground state of the time dependent linear potential. Then,  $\phi(x, t)$  would be approximately equal to the first term in equation 43 with  $b$  replaced by  $b\gamma(\gamma-1)t^{\gamma-2}/2$ . Thus, one would expect that the contribution from  $\phi$  to  $f(t)$  is utmost of the order  $\exp[t^{(2\gamma-1)/3}]$ . From equation 52, we then conclude that

$$\alpha = \frac{-b^2 \gamma^2}{2D(2\gamma-1)}. \quad (53)$$

We now compare the above heuristic result for  $\alpha$  with results from numerical simulations (with  $D = 1$ ). It turns out that it is more convenient to numerically measure the survival probability  $S(t)$  rather than directly measure  $f(t)$ .  $S(t)$  is the probability that a random walker has not crossed the barrier up to time  $t$  and is related to  $f(t)$  by  $f(t) = -dS(t)/dt$ ; hence it has the same  $\alpha$  as  $f(t)$ . To estimate  $\alpha$  we need to go to large times, but then face the problem that  $S(t)$  becomes exponentially small. It is difficult to overcome this problem using conventional Monte Carlo methods. Instead, we use an algorithm known as “go with the winners” algorithm (Grassberger 2002). We briefly describe the algorithm. We start with  $N$  ( $N = 2 \times 10^5$  in our case) random walkers at the origin. When the number of walkers get reduced by half (due to absorption at the boundary), copies are made of the remaining surviving ones, and the survival probability is halved. By repeating this procedure, we can go down to very low values of survival probability keeping the number of live walkers constant. As an example of the kind of data that is obtained, we show the survival probability for  $\gamma = 0.75$  in figure 8.

From the numerical results for the survival probability,  $\alpha$  is determined by best fit. In figure 9 we show the variation of  $\alpha$  with  $\gamma$ . The data agrees well with the formula in equation 53. We would expect that equation 53 is an exact result.

## 6 HALO MASS FUNCTION FROM $N$ -BODY SIMULATIONS

A two parameter empirical formula for the halo mass function as given in Sheth & Tormen (1999) can be written as

$$\nu f(\nu) = A \sqrt{\frac{q\nu}{2\pi}} [1 + (q\nu)^{-p}] \exp\left(-\frac{q\nu}{2}\right). \quad (54)$$

Here  $\nu = \delta_{sc}(z)^2 / \sigma^2(m)$ . The parameters are  $q = 0.707$ ,  $p = 0.3$  and  $A \approx 0.322$ , which is set by enforcing the condition that integral of  $f(\nu)$  over all  $\nu$  equals unity. The Press Schechter formula has  $q = 1$ ,  $p = 0$  and  $A = 1/2$ . For small  $\nu$  one obtains  $\nu f(\nu) \propto \nu^{0.5-p}$ . Equivalently for large  $t$ ,  $f(t) \propto t^{3/2-p}$ .

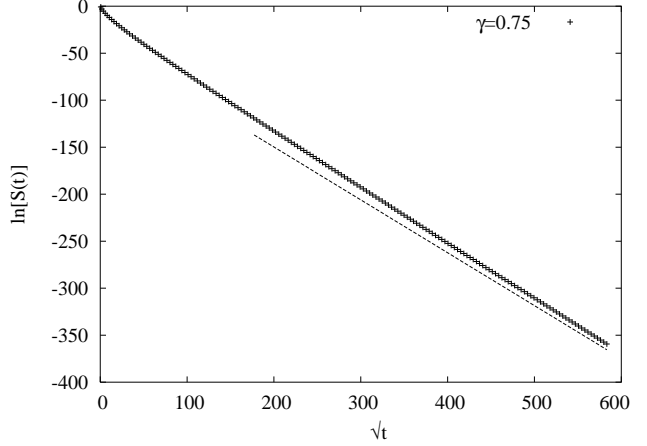


**Figure 8.** The variation of the logarithm of the survival probability  $S(t)$  with  $\sqrt{t}$  is shown. The dotted line has slope as in equation 53 and is shown for comparison. Very small  $S(t)$  can be reached using specialised algorithms.

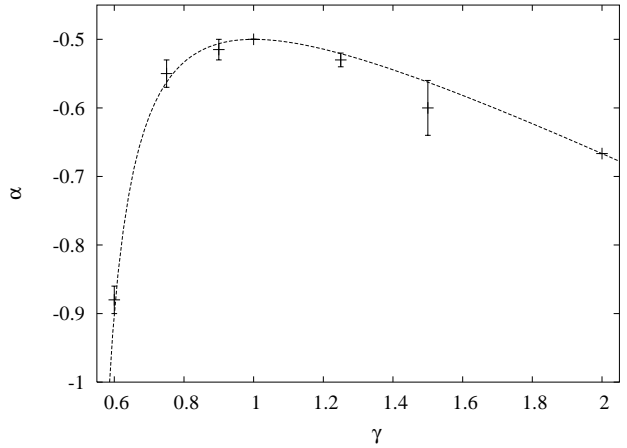


**Figure 9.** The variation of  $\alpha$  with  $\gamma$  is shown. The values for  $\gamma = 1$  and  $\gamma = 2$  are exact. The data is for  $b = 1.0$ . The solid line is the formula in equation 53.

In this section we fit the  $N$ -body mass function with the unconditional mass function for the square root barrier, taking  $b$  and  $q$  as free parameters (see equation 4). For this, we use the small time asymptotic form of the unconditional mass function as given in equation 33. We use the halo catalogues of GIF simulations for  $\Lambda$ CDM cosmology, as available on <http://www.mpa-garching.mpg.de/Virgo/>. The cosmological parameters for the simulation are  $\Omega_m = 0.3$ ,  $\Omega_\Lambda = 0.7$ ,  $h = 0.7$  and  $\sigma_8 = 0.9$ . The box size of these simulations was  $L = 141 h^{-1} \text{Mpc}$  and a total of  $256^3$  particles were simulated. We only consider haloes with at least 50 particles and a maximum mass of  $3 \times 10^{14} M_\odot$ . This upper limit is chosen as the statistics of haloes with masses  $\gtrsim 3 \times 10^{14} M_\odot$  is dominated by significant noise. For lower halo mass limit one should typically consider  $\gtrsim 70$  particles (Arif Babul private communication). The best-fit value of the parameters we obtain are  $b \approx 0.5$  and  $q \approx 0.55$ . This value of  $q$  is somewhat smaller than that obtained by fitting the expression 54. Interestingly, using the large time

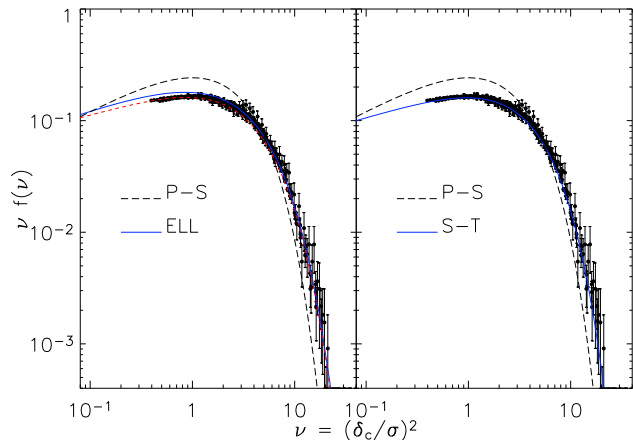


**Figure 10.** The halo mass function. Filled circles show the mass function obtained from GIF simulations. The error bars show the poissonian error. *Left panel:* The dashed curve shows the Press Schechter mass function and the solid curve shows the moving barrier mass function (see section 6 for details). The dotted curve shows the asymptotic form of the unconditional mass function (equation 33). *Right panel:* The solid curve shows the best-fit empirical mass function obtained in Sheth & Tormen (1999).

behaviour of  $f(t)$  as discussed in section 3.2, for  $b = 0.5$  one obtains  $f(t) \propto t^{3/2-p'}$ , where  $p' \approx 0.2$ . In the following analysis we restrict to our best-fit values for  $q$  and  $b$ .

In figure 10, the left panel shows the GIF mass function (filled circles) and the solid curve shows the mass function as given in equation 30. Also plotted for comparison is the Press Schechter mass function (dashed curve) and the asymptotic form of mass function as given by equation 33 (dotted curve). In the figure we have labelled the square root barrier mass function as ‘ELL’ as in ellipsoidal collapse. The fact that the full solution gives a worse fit than the asymptotic formula (with the same parameters) shows the danger in fixing parameters through approximate formulae.

The right panel shows the Sheth & Tormen (1999) mass function as given by equation 54. It can be seen that the square root barrier mass function gives a reasonable description of the halo mass function obtained from the simulations. It also shows the difficulty of extracting the correct  $\gamma$  from the simulations. To do so, one needs to have good data for small mass, and the resolution at these mass scales is not good enough.

## 7 IMPLICATIONS FOR MERGING HISTORY OF HALOES

In this section, we present an application of our calculation. We use the results of the conditional mass distribution for the square root barrier to estimate the major merger rates of dark matter haloes. In simple models (Wyithe & Loeb 2002, 2003; Mahmood, Devriendt & Silk 2004), halo mergers are followed by galaxy mergers. Major mergers of galaxies are thought to trigger off quasars. Thus halo merger rates provide an estimate of quasar numbers at any given redshift. This is particularly useful, since quasars can be observed directly up to sufficiently high redshifts ( $z \gtrsim 6$ ). Previous studies have shown that the Press-Schechter (PS)

halo major merger rates are consistent with the evolution of quasars at high redshifts ( $z \gtrsim 2$ ) but fail for low redshifts (Wyithe & Loeb 2002). The low redshift evolution of quasars is marked by an enhanced role of baryonic components and is therefore probably beyond the reach of simple predictions based on halo major merger rates.

In the PS model the simplest estimates of halo ‘creation’ rates are often taken as the positive term in the cosmological-time (or redshift) derivative of the unconditional halo mass function (we explicitly write cosmological-time so as to avoid any confusion with the notation  $t, t_0, t_1, t_2$  used in the paper). This is partly a necessity as in the PS formalism all haloes are continuously accreting matter and are therefore newly formed. There is no direct way of differentiating between minor and major accretion episodes. To counter this deficiency of the model, a simple argument is used to define a major merger: the haloes which accrete mass comparable to their own mass, in a short interval of time are said to undergo a major merger. Using the conditional mass function, therefore, one can compute the probability that at a very small look back time  $\Delta a$ , a given halo had a ‘formed’ progenitor less than half of its present mass. Substituting  $\Delta a$  by  $da/d\tau$  (where  $\tau$  is the cosmological time), in this probability yields the rate at which haloes of a given present day masses are forming through major mergers. We call these rates as major merger rates of haloes. This approach has been discussed, for e.g., in Mahmood, Devriendt & Silk (2004).

Alternatively instead of looking back-wards one can compute the probability that a given halo merges with a comparable mass object (‘formed’ or otherwise) during a small step  $\Delta a$  forward in time (Wyithe & Loeb 2003). The two approaches yield essentially similar results.

### 7.1 ‘Creation’ rates

We first consider the implications of taking the positive term in the cosmic-time derivative of the unconditional mass function. The left panel in figure 11 shows the redshift evolution of creation rates as obtained from the Press Schechter mass function (dashed curve) and the mass function for the square root barrier (solid curve). These rates have been integrated over the minimum masses as depicted in the figure. It can be seen that the moving barrier mass function gives considerably higher creation rates for large redshifts.

### 7.2 Major merger rates

In order to compute major merger rates of haloes, we consider an object with a given  $t_1$  (corresponding to mass  $M_1$ ) at some epoch; for a small look back time  $\Delta a \rightarrow 0$ , we can apply the result of equation 37 to obtain  $f(t_2|t_1)$ . The fraction of objects with less than half mass progenitors can therefore be computed as

$$\begin{aligned}
 w(t_2 > t_h | t_1) &= \int_{t_h}^{\infty} dt_2 f(t_2|t_1) \\
 &= \frac{\Delta a}{\sqrt{D}t_1} \sum_v \frac{1}{v} \left(\frac{t_1}{t_h}\right)^{v/2} \frac{U'_v(-b/\sqrt{D})^2}{I_v(-b/\sqrt{D})}, \quad (55)
 \end{aligned}$$

where  $t_1 \equiv S(M_1)$  and  $t_h \equiv S(M_1/2)$ . Replacing  $\Delta a$  by  $\dot{a} = da/d\tau$  gives us  $\dot{w}$ . This represents the fraction of ob-

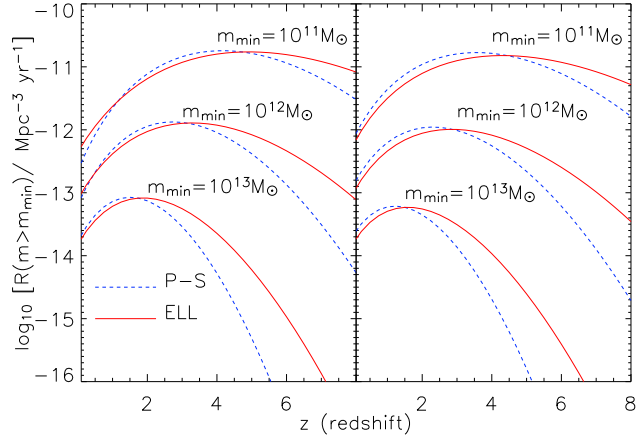


**Figure 11.** *Left Panel:* The cumulative creation rates of haloes with minimum masses as depicted in the figure. *Right panel:* The cumulative major merger rates of haloes, above some given masses (see section 7.2 for details).

jects of mass  $M_1$  formed from major mergers, per unit time. Multiplying  $\dot{w}$  with the existing number of objects of mass  $M_1$  as determined from the mass function, gives the ‘major merger rate’ of haloes of mass  $M_1$ . Integrating the rate over  $M_1$  from some minimum mass  $M_{min}$  to  $\infty$  gives the cumulative major merger rate of objects above mass  $M_{min}$ .

In the right panel of figure 11 we plot cumulative major merger rates of haloes in the constant barrier (dashed curve) Press Schechter model and the moving barrier (solid curve) model. For the moving barrier model the unconditional mass function is as given by equation 33. Figure 11 shows that the moving barrier model yields a higher number of cumulative major merger rates towards high redshifts and particularly so for massive haloes ( $\sim 10^{12-13} M_\odot$ ). This is precisely the halo mass range which is relevant for quasars. The inclusion of moving barrier threshold could, therefore, significantly affect the predictions of analytic and semi-analytic models dealing with the evolutionary history of the high redshift quasars.

As an example we compute the number counts of quasars above a given redshift and flux level in observed soft (0.5 – 2 keV) and hard (2 – 10 keV) X-ray bands. For this, we use the model discussed in Mahmood, Devriendt & Silk (2004). The black hole mass ( $M_{BH}$ ) to halo mass ( $M_h$ ) relation is as described in that paper. The major merger rates of haloes are computed as discussed above. Using the  $M_{BH} - M_h$  relation these rates are converted into black hole formation rates. The bolometric luminosities are estimated as the Eddington luminosity for a given black hole mass. To obtain the luminosity in observed X-ray bands, at a given redshift  $z$ , we derive bolometric corrections in bands  $0.5(1+z) - 2(1+z)$  keV and  $2(1+z) - 10(1+z)$  keV respectively. For this we use the spectral energy distribution and the rest-frame bolometric corrections described in Marconi et al. (2004). The quasar life times are taken as the local dynamical times of galaxies (note that the relative difference between the Press Schechter and the moving barrier model will be independent of the lifetime). Thus luminosity functions in  $0.5(1+z) - 2(1+z)$  keV and  $2(1+z) - 10(1+z)$  keV bands are obtained.

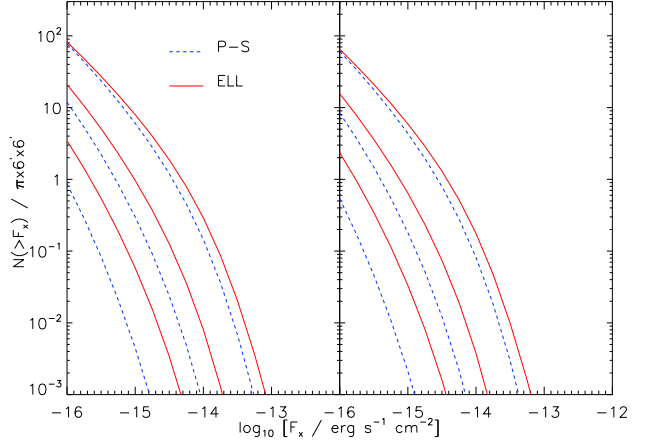


**Figure 12.** *Left panel:* The number count of quasars in the observed hard X-ray band (2 – 10 keV). In each line style, the set of three curves from top to bottom correspond to  $z \gtrsim 3, 5$  and 7 respectively. Solid curves show the moving barrier prediction and dashed curves show the prediction of Press Schechter model. *Right panel:* The number count of quasars in the observed soft X-ray band (0.5 – 2 keV).

Quasar luminosities are related to the observed flux as  $F_X(L_X, z) = L_X/4\pi/D_L(z)^2$  (here  $L_x$  is the X-ray luminosity). From the luminosity function  $\phi(L_X, z)$  of quasars, the number of X-ray quasars in the whole sky, above some flux level  $F_X$  and above some redshift  $z$  is given as (Haiman & Loeb 1998)

$$N(> F_X, > z) = 4\pi \int_z^\infty dz' \int_{L(F_X, z')}^\infty dL_X \left( \frac{d^2V}{dz'd\Omega} \right) \phi(L_X, z). \quad (56)$$

Here  $d^2V/dz/d\Omega$  is the comoving volume element per unit redshift and per unit solid angle. The left panel of figure 12 shows the number count in a  $6'$  circle, for hard X-ray band. The right panel depicts the results for soft X-ray band. The solid curve is the moving barrier model prediction and the dashed curve is the Press Schechter prediction. It can be seen that there is a pronounced discrepancy between the two models at high redshifts. Even though the full nature of this discrepancy can only be known through a model based on  $N$ -body merger trees, our results highlight the difference qualitatively. It may be added here that the difference in the models primarily owes to the difference in the halo mass function in the two models.

## 8 SUMMARY AND DISCUSSION

In this paper we studied the first crossing probability  $f(t)$  of one dimensional random walks across a barrier moving as  $t^\gamma$ . Complete analytical solutions for the square root barrier ( $\gamma = 1/2$ ) and the quadratic barrier ( $\gamma = 2$ ) were presented. For arbitrary power law barriers, large time estimates of the first crossing probability were derived. We showed that the formula for  $f(t)$  as presented in Sheth & Tormen (2002) is not valid for general  $\gamma$ . We also presented a methodology for approaching the two barrier problem for conditional mass function of haloes. This is relevant for deriving the progenitor distribution of haloes. Unlike the stationary and

the linear barrier, the conditional first crossing probability does not follow a simple re-scaling of the unconditional first crossing probability for other barrier forms.

In Sheth, Mo & Tormen (2001), it was argued that  $\gamma \approx 0.6$  is the barrier arising from ellipsoidal collapse. It was also shown the mass function from  $N$ -body simulations could be fitted well by a barrier of this kind. In this paper, we fitted the  $N$ -body data using the square root barrier. This barrier has the advantage of being analytically tractable and the conditional distributions are also fully known. As shown in section 6, the numerical data is fitted well with the square root barrier too. Since we also derived large time behaviour of first passage distributions across barriers with arbitrary  $\gamma$ , one could ask the following question. Treating  $\gamma$  as a free parameter, can it be determined using the data from  $N$ -body simulations? For small times (large masses),  $f(t)$  is dominated by the stationary barrier. It is only for large times that  $\gamma$  plays a role. Thus, to determine  $\gamma$ , the  $N$ -body simulations should have good resolution at small masses. This is currently not available, and it is not possible to determine  $\gamma$  from the simulations with any degree of confidence.

We also compared the predictions for merger rates of haloes in the constant barrier model with that of the moving barrier model. The moving barrier model predicts a significantly higher merger rates for massive haloes towards high redshifts. This arises as a consequence of the fact that the moving barrier mass function yields more massive haloes at high redshifts, as compared to the standard Press Schechter mass function. In this regard an interesting exercise would be to compare the halo merger rates obtained from simulations with the constant and the moving barrier merger rates. In the present context it appears that the prediction of the moving barrier model is consistent with the early formation of massive galaxies (Glazebrook et al. 2004) and the presence of high redshift quasars with massive host haloes (Fan et al. 2003). We also presented a calculation of X-ray quasar number count above a given flux level and a given redshift. In terms of relative abundances, we found that the moving barrier model predicts systematically more quasars towards higher redshift. At  $z \gtrsim 6$  the number reaches almost double the standard Press-Schechter prediction.

van den Bosch (2002) has shown that there is a difference between the average mass accretion history of haloes in simulations and that derived from the semi-analytic merging history trees (Somerville & Kolatt 1999). In particular the  $N$ -body simulations suggest an earlier formation of haloes than is inferred from semi-analytic trees. Earlier formation epochs are reminiscent of higher merging activity towards high redshifts, which is the case in the moving barrier model. In this context it is worth pointing out that our expressions for conditional mass function could be used to generate “improved” merging history trees. The form of equation 34 suggests that the task of drawing progenitors using the given expression may not be as easy as in the case of a constant barrier model. However, the analysis in section 3.4 indicates that when  $\Delta a/\sqrt{t_1} \rightarrow 0$  one can use a considerably simplified expression for the conditional distribution  $f(t_2|t_1)$  (equation 37). Therefore, for a given present day halo with mass  $M_1$  (corresponding to  $t_1$ ) one can choose an appropriately small  $\Delta a$  and use equation 37 to draw the progenitor masses. Alternatively we have pointed out that the two opposite limits for the conditional mass function are the con-

stant barrier distribution and the distribution obtained by simple re-scaling of the unconditional mass function. Hence the merging history trees in the moving barrier model would be constrained by these limiting distributions. In a forthcoming work this issue will be investigated in further detail.

## ACKNOWLEDGEMENTS

The research of AM at Oxford was supported by the Eddie Dinshaw foundation, Balliol College. RR was supported by NSF grant DMR-0207106. We would like to thank Joe Silk, Julien Devriendt and James Taylor for their useful comments on the present work. We are grateful to Alessandro Marconi for explaining the k-corrections for quasars. We also thank Adrian Jenkins and Ravi Sheth for discussing various aspects of halo mass function in  $N$ -body simulations, and Alexander Knebe and Darren Reed for making available the outputs from their  $N$ -body simulations for comparison.

## REFERENCES

- Bardeen J. M., Bond J. R., Kaiser N., Szalay A. S., 1986, ApJ, 304, 15 (BBKS)
- Bender C. M., Orszag S. A., *Advanced Mathematical Methods for Scientists and Engineers*, 1978, McGraw-Hill Book Company, New York
- Bond J. R., Cole S., Efstathiou G., Kaiser N., 1991, ApJ, 379, 440 (BCEK)
- Doroshkevich A. G., 1970, *Astrofizika*, 3, 175
- Del Popolo A., Gambera M., 1998, A&A, 337, 96
- Del Popolo A., 2002, MNRAS, 337, 529
- Erdelyi A., ed., *Higher Transcendental Functions*, Volume 2, 1953, McGraw-Hill Book Company, New York
- Fan X., et al., 2003, *Astron. J.*, 125, 1649
- Feller W., *An introduction to probability theory and its applications*, 1970, Wiley, New York
- Gelb J., Bertschinger E., 1994, ApJ, 436, 467
- Glazebrook K., et al., 2004, *Nature*, 340, 181
- Grassberger P., 2002, *Comp. Phys. Commun.*, 147, 64
- Haiman Z., Loeb A., 1998, ApJ, 503, 505
- Jenkins A., Frenk C. S., Pearce F. R., Thomas P. A., Colberg J. M., White S. D. M., Couchman H. M. P., Peacock J. A., Efstathiou G., Nelson A. H., 1998, ApJ, 499, 20
- Jenkins A., Frenk C. S., White S. D. M., Colberg J. M., Cole S., Evrard A. E., Couchman H. M. P. & Yoshida N., 2001, MNRAS, 321, 372
- Kauffmann G., White S. D. M., Guiderdoni B., 1993, MNRAS, 264, 201
- Krapivsky P. L., Redner S., 1996, *Am. J. Phys.*, 64, 546.
- Lacey C., Cole, S., 1994, MNRAS, 271, 676
- Lacey C., Cole, S., 1993, MNRAS, 262, 627
- Mahmood A., Devriendt J. E. G., Silk J., preprint (astro-ph/0401003)
- Marconi A., Risaliti G., Gilli R., Hunt L.K., Maiolino R., Salvati M., 2004, MNRAS, 169, 185
- Mo H. J. & White S. D. M., 1996, MNRAS, 282, 347
- Monaco P., 1997a, ApJ, 287, 753
- Monaco P., 1997b, ApJ, 290, 439
- Press W. H. & Schechter P., 1974, ApJ, 187, 425
- Sheth R. K., Tormen G., 1999, MNRAS, 308, 119

Sheth R. K., Lemson G., 1999, MNRAS, 304, 767  
 Sheth R. K., Mo H. J., Tormen G., 2001, MNRAS, 323, 1  
 Sheth R. K., Tormen G., 2002, MNRAS, 329, 61  
 Somerville R., Kolatt T. S., 1999, MNRAS, 305, 1  
 Tormen G., 1998, MNRAS, 297, 648  
 van den Bosch F., 2002, MNRAS, 331, 98  
 Wyithe J. S. B., Loeb A., 2002, ApJ, 581, 886  
 Wyithe J. S. B., Loeb A., 2003, ApJ, 595, 614

large  $v$  asymptotic form of the function  $U_v(y)$  and obtain the final integral as

$$I_v(-b/\sqrt{D}) = \pi\sqrt{v} \left(\frac{v}{e}\right)^v \left[1 + \frac{b}{\pi\sqrt{vD}} + O(1/v)\right]. \quad (\text{A8})$$

## APPENDIX A: PARABOLIC CYLINDER FUNCTIONS

In this appendix, we discuss some standard results pertaining to parabolic cylinder functions and their integrals. Parabolic cylinder functions are the solutions of the differential equation 22. An integral representation of these functions for  $v \geq -1$  is given as (Erdelyi 1953)

$$U_v(x) = \sqrt{\frac{2}{\pi}} e^{x^2/4} \int_0^\infty dt e^{-t^2/2} t^v \cos\left(xt - \frac{v\pi}{2}\right). \quad (\text{A1})$$

For large  $v$ , the asymptotic form of these functions is

$$U_v(x) = \sqrt{2} \left(\frac{v}{e}\right)^{v/2} \left[ \cos\left(x\sqrt{v} - \frac{v\pi}{2}\right) + \frac{x(x^2 - 6)}{24\sqrt{v}} \sin\left(x\sqrt{v} - \frac{v\pi}{2}\right) + O(1/v) \right]. \quad (\text{A2})$$

For the problem discussed in the paper, the boundary condition is  $U_v(-b/\sqrt{D}) = 0$ . For large  $v$ , we can keep just the first term in equation A2 and estimate the eigenvalues to be given by

$$\frac{\pi v}{2} + \frac{b\sqrt{v}}{\sqrt{D}} = (2n + 1)\frac{\pi}{2}, \quad (\text{A3})$$

where  $n$  is a large positive integer. Solving, we obtain

$$v_n = 2n - \frac{2\sqrt{2}b}{\pi\sqrt{D}}\sqrt{n} + \frac{2b^2}{\pi^2 D} + (2k - 1) + O\left(\frac{1}{\sqrt{n}}\right). \quad (\text{A4})$$

Here,  $k$  is an arbitrary integer.

To compute the asymptotic behavior of  $U'_v(x)$  we note the recursion relation  $2U'_v(x) = xU_v(x) - 2U_{v+1}(x)$ . Thus for  $x = -b/\sqrt{D}$  we have  $U'_v(-b/\sqrt{D}) = -U_{v+1}(x)$ . Using equation A2 we can then write the large  $v$  asymptotic form for  $U'_v(-b/\sqrt{D})$  as

$$U'_v\left(\frac{-b}{\sqrt{D}}\right) = \sqrt{2v} \left(\frac{v}{e}\right)^{v/2} \sin\left(\frac{v\pi}{2} + \frac{b\sqrt{v}}{\sqrt{D}}\right) [1 + O(1/v)]. \quad (\text{A5})$$

In order to compute the large  $v$  asymptotic form of the integral  $I_v(-b/\sqrt{D})$  we first note that (Erdelyi 1953)

$$\int_0^\infty U_v^2(y) dy = \frac{\sqrt{\pi}}{2^{3/2}} \left[ \frac{\psi(1/2 - v/2) - \psi(-v/2)}{\Gamma(-v)} \right], \quad (\text{A6})$$

where  $\Gamma(x)$  is a gamma function and  $\psi(x)$  is a logarithmic derivative of the gamma function, defined as  $\psi(x) = \Gamma'(x)/\Gamma(x)$ . Using a set of standard results [for e.g. given in the appendix of Bender & Orszag (1978)] we obtain the large  $v$  behavior of this integral as

$$\int_0^\infty U_v^2(y) dy = \pi\sqrt{e} \left(\frac{v}{e}\right)^{v+1/2} [1 + O(1/v)]. \quad (\text{A7})$$

Now in the remaining integral  $\int_{-b/\sqrt{D}}^0 U_v^2(y) dy$  we use the